

Neutron Matter from Low to High Density

STEFANO GANDOLFI,¹ ALEXANDROS GEZERLIS,² J. CARLSON¹

¹*Theoretical Division, Los Alamos National Laboratory, Los Alamos, NM 87545, USA; email: carlson@lanl.gov, stefano@lanl.gov*

²*Department of Physics, University of Guelph, Guelph, ON, N1G 2W1, Canada; email: gezerlis@uoguelph.ca*

Key Words superfluidity, neutron stars, strongly correlated matter, nuclear forces

Abstract Neutron matter is an intriguing nuclear system with multiple connections to other areas of physics. Considerable progress has been made over the last two decades in exploring the properties of pure neutron fluids. Here we begin by reviewing work done to explore the behavior of very low density neutron matter, which forms a strongly paired superfluid and is thus similar to cold Fermi atoms, though at energy scales differing by many orders of magnitude. We then increase the density, discussing work that ties the study of neutron matter with the determination of the properties of neutron-rich nuclei and neutron-star crusts. After this, we review the impact neutron matter at even higher densities has on the mass-radius relation of neutron stars, thereby making contact with astrophysical observations.

CONTENTS

INTRODUCTION	2
VERY LOW DENSITIES: NEUTRON MATTER AND COLD ATOMS	3
<i>Interaction and Equation of State</i>	4
<i>Superfluid Pairing</i>	6
MODERATE DENSITIES: INTERACTIONS AND EQUATION OF STATE	8
<i>Neutron-Neutron Interaction</i>	8
<i>Equation of State</i>	12
<i>Three Nucleon Interactions</i>	14
INHOMOGENEOUS NEUTRON MATTER	15
<i>Neutron Matter and Density Functionals</i>	16
<i>Neutron Drops</i>	16

HIGHER DENSITIES: NEUTRON MATTER AND NEUTRON STARS	18
<i>Equation of State</i>	18
<i>Neutron Star Mass/Radius</i>	23
CONCLUSIONS AND OUTLOOK	25

CONTENTS

1 INTRODUCTION

The properties of neutron matter have long been recognized as critical to the properties of neutron-rich nuclei and neutron stars. Low-density neutron matter critically impacts our understanding of neutron-rich nuclei. Similarly the equation of state of high-density low-temperature matter is critical in determining the properties of neutron stars, including the mass-radius relationship and the neutron-star maximum mass.

During the past few years interest in neutron matter have been resurgent for several reasons. At very low densities, neutron matter is very similar to cold Fermi atoms near unitarity (infinite scattering length), since two free neutrons are very nearly bound. This enables stringent tests of theories of fermions in this strongly-interacting regime (1). The equation of state (2,3) and pairing gap of unitary fermions (4,5,6) have been calculated precisely and measured very accurately. These experiments provided severe tests of the theories; some of the calculations (including those reviewed here) provided excellent predictions while others were less successful.

There has also been a resurgence of interest in the properties of neutron-rich nuclei. New facilities, such as FRIB, will probe the properties of many hitherto inaccessible nuclei. Among the several expected discoveries, the history of nucleosynthesis could be mentioned: we still do not know where the heavy elements were created. (7) Such experiments will probe the extreme isospin-imbalance limit, thereby informing nuclear models and ab initio approaches. Typically density functionals (8) are used to predict the properties of these nuclei; while some components of the density functional are very tightly constrained from stable nuclei the extreme isospin limit is less constrained. Many-body calculations of inhomogeneous neutron matter can provide further constraints on the parameters entering density functionals. This is also important for the inner crust of neutron stars, where inhomogeneous neutron matter fills the space between the lattice of heavy neutron-rich nuclei.

Finally, neutron stars have become even more important in recent years. The discovery of the first two-solar-mass neutron stars (9,10) provided critical constraints on the dense matter equation of state. These observations eliminated whole classes of models. Combined with the recent observations of massive neutron stars, the attractive nature of the neutron-neutron interaction at low momenta means the equation of state must be soft at low density with a rapid transition to a high-pressure when the higher-momentum neutron-neutron and

three-neutron interactions become important.

Astrophysical observations are providing better constraints on the whole mass-radius relation of dense matter, which is critical to a real understanding of neutron stars (11, 12, 13, 14). In addition, neutron-star mergers are increasingly seen as an important site for heavy-element synthesis, providing even more important reasons for understanding the properties of neutron-rich matter. In the near future, we can look forward to the observation of gravitational waves from these neutron-star mergers (15), providing the most direct evidence of the structure of neutron matter and neutron stars.

2 VERY LOW DENSITIES: NEUTRON MATTER AND COLD ATOMS

At very low densities the equation of state of neutron matter is determined by the s-wave (spin-0, isospin-1) neutron-neutron interaction. This interaction is very attractive, almost large enough to produce a bound di-neutron. The neutron-neutron scattering length is -18.5 fm (16, 17), much larger than typical nuclear scales; the neutron-neutron effective range is about 2.7 fm.

Bertsch had proposed a model of low-density neutron matter that was simply a zero-range interaction tuned to infinite scattering length (18), now called the unitary limit in cold atom systems. Remarkably, experiments in cold atom systems shortly thereafter provided constraints on the properties of the unitary Fermi gas (and therefore also indirectly of low-density neutron matter). The relevant parameter in these strongly interacting low-density systems is the Fermi momentum $k_F = (3\pi^2\rho)^{1/3}$, where ρ is the number density, times the scattering length a ; in the limit that the scattering length goes to infinity all properties of the system are fundamental constants times the corresponding free Fermi gas quantity. The equation of state in this limit is characterized by the Bertsch parameter ξ :

$$E = \xi E_{FG} = \xi \frac{3}{5} \frac{\hbar^2}{2m} k_F^2, \quad (1)$$

where E_{FG} is the energy of a two-component free Fermi Gas at number density ρ . Similarly the superfluid pairing gap is characterized by the ratio δ of the gap in the unitary limit to the Fermi energy of the non-interacting system:

$$\Delta = E(N+1) - \frac{1}{2}[E(N) + E(N+2)] = \delta E_F = \delta \frac{\hbar^2}{2m} k_F^2. \quad (2)$$

Several properties of the unitary Fermi gas have been studied both theoretically and experimentally. This is a very strongly correlated system, with a pairing gap of the order of the Fermi energy ($\delta \approx 1$), unlike traditional superconductors (where $\delta \approx 10^{-4}$). We concentrate in this section on comparisons of the equation of state and superfluid pairing gaps of cold atoms and neutron matter. While neutron matter is much more complicated, with a significant effective range and spin-dependent interactions that give small but finite corrections at low density, important similarities remain between the two systems. A detailed review of pairing in neutron matter can be found in (19), while comparisons to cold atom physics can be found in (20, 21).

2.1 Interaction and Equation of State

The equation of state is in a sense the most fundamental property of neutron matter. At low densities, as we have described, it can be related to the properties of cold atoms, which have a tunable scattering length and an effective range that is nearly zero compared to the average interparticle spacing. Neutron matter, in contrast, has a fixed scattering length and effective range. They can be compared to cold atoms by comparing systems at the same scattering length times Fermi wave number, $k_F a$, as well as the same effective range times Fermi wave number, $k_F r_e$, (i.e. by using dimensionless parameters characterizing the low-density system).

The equation of state for neutron matter and cold atoms have been compared in Quantum Monte Carlo calculations (20, 22). For cold atoms we assume a nearly zero-range interaction tuned to give the same scattering length times Fermi momentum as neutron matter. The details of the interaction are not important as long as we are at low density.

For neutron matter various simple interactions have been considered. The simplest is a pure s-wave interaction that acts only in relative s-waves, as these are the dominant interactions at low density (see the discussion in Section 3.1 below). The potential is adjusted to have the same scattering length and effective range as that inferred from the neutron-neutron interaction (which is, in general, active in higher partial waves). We also consider a more realistic interaction that contains both s- and p-wave interactions (23) as the latter start to become relevant at higher densities. These simple interactions include all the physics required for the study of low-density matter, but at higher densities (and hence higher Fermi momenta) the full neutron-neutron and three-neutron interactions must be considered.

At low density neutron matter is a very strongly paired superfluid, requiring the inclusion of pairing into a realistic treatment of even the equation of state. These calculations calculate the ground state through Quantum Monte Carlo methods, specifically Diffusion Monte Carlo. They project out the ground state through:

$$|\Psi_0\rangle = \exp(-H\tau)\Psi_T = \prod_{i=1}^N \exp\left(-H \frac{\tau}{N}\right) |\Psi_T\rangle, \quad (3)$$

where we take the limit of large τ to reach the ground state and Ψ_T is an approximate trial wave function for the system. In this case we take the trial wave function to be of a BCS-Jastrow form:

$$|\Psi_T\rangle = \left[\prod_{i<j} f(r_{ij}) \right] \mathcal{A} \left[\prod_{i,j} \phi(r_{ij}) \right], \quad (4)$$

where $\phi(r)$ is an s-wave pairing function describing the pairing of spin up and spin down neutrons, and the Jastrow function f can be used to adjust the short-range behavior of the wave function independently of the superfluid pairing. For the appropriate choice of $\phi(r)$, this wave function reduces to the standard Jastrow-

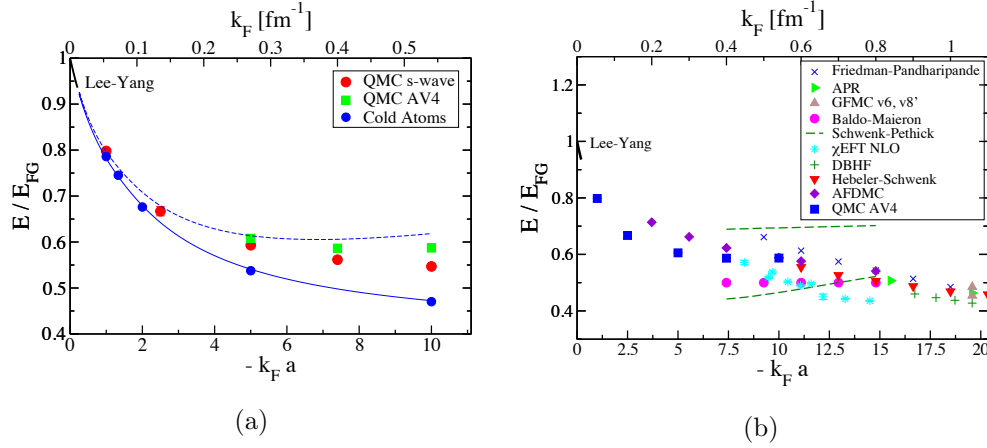


Figure 1: The equation of state of low-density neutron matter compared to that of cold atoms at the same value of Fermi momentum times scattering length ($k_F a$). The left side compares cold atoms and neutron matter (see text), and the right panel shows neutron matter results for different methods over a wider range of $k_F a$. Figures taken from (21,22).

Fermi Gas wave function. The radial form of the function $\phi(r)$ and $f(r)$ are determined in variational calculations.

These calculations have a fixed-node approximation that implies they provide variational upper bounds to the true energy. They have proven to be very accurate in studies of cold atom systems, where accurate lattice calculations without a fixed-node approximation are available (3). These calculations are also in very good agreement with cold atom experiments (2).

The results of the equation-of-state calculations are shown in Fig. 1. The left panel compares neutron matters and cold atoms at very low density. The vertical axis indicates the ratio of fully interacting energy to the energy of the free Fermi gas at the same density, the horizontal axis is the Fermi momentum times the scattering length $k_F a$; on the upper axis the equivalent Fermi momentum for neutron matter is indicated. At extremely low densities, or equivalently small value of $k_F a$, analytic results are available (24,25), and the higher-order Lee-Yang result is plotted as a line in the figure.

Results for cold atoms with zero effective range are plotted as filled blue circles, in the limit of infinite $k_F a$ these should approach 0.37. Cold atom results for the dependence on the effective range are also available, the equation of state can be expanded in terms of k_F :

$$E/E_{FG} = \xi + \mathcal{S} k_F r_e + \dots, \quad (5)$$

where $\mathcal{S} = 0.12(3)$ is a universal constant that has been determined in the lattice calculations and in Diffusion Monte Carlo (3,26). Using the above equation of including the experimental neutron-neutron effective range r_e gives the dashed line in the figure.

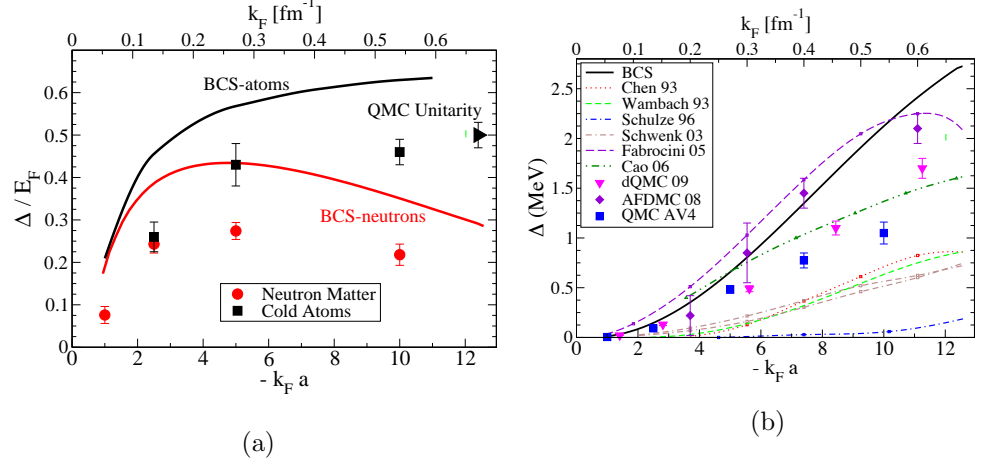


Figure 2: The pairing gap of low-density neutron matter compared to that of cold atoms at the same value of Fermi momentum times scattering length (left). Comparison of different calculations of the neutron matter gap (right). Figures taken from (20, 22).

The calculations of neutron matter with the spin singlet s-wave interaction from AV18 gives the solid red points, correcting the p-wave interactions from AV4 gives the green squares. At very low densities all these calculations are very similar. At slightly higher densities the correction from the p-wave interaction is slightly repulsive, and is in good agreement with the effective range expansion above.

The right panel shows a comparison of various methods for the neutron matter equation of state over a somewhat wider range of densities. Methods include Fermi Hypernetted chain resummation techniques (27, 28), the Brueckner-Bethe-Goldstone expansion (29), effective field theory (30) and several Quantum Monte Carlo methods including Green's function Monte Carlo (31) and Auxiliary field diffusion Monte Carlo (32, 33). All the calculations are in reasonable agreement, indicating a soft neutron matter equation of state at low density.

2.2 Superfluid Pairing

Neutron pairing at low density is important in both neutron-rich nuclei and in the crust of neutron stars. Pairing in nuclei and matter has been a long-studied topic, see a review by Dean and Hjorth-Jensen (34). For pairing at low density, recent work in cold atom systems, both theoretical and experimental, has advanced our understanding of pairing in the strongly superfluid regime. Experiments and calculations indicate that the pairing gap in neutron matter is quite substantial, reaching a peak of approximately 30 per cent of the Fermi energy. This is the largest Fermion pairing gap known in nature, and only slightly smaller than the 45 per cent pairing found in cold atoms at unitarity (4, 5, 6).

The pairing gap for matter can be calculated by computing the energy of

even and odd particle systems and extrapolating to the thermodynamic limit. For traditional superfluids and superconductors this is extremely difficult as the small value of the pairing gap implies a very large coherence length, in principle requiring extremely large simulations with very small differences in energy. For this reason Quantum Monte Carlo methods had not previously been used to extract superfluid pairing gaps.

Analytic techniques, are, of course available. In nuclear physics the BCS equations have often been used to study pairing in neutron matter. At low densities the s-wave pairing predictions from BCS theory are mostly independent of nuclear interaction models because the interaction is very well constrained at low momenta. However corrections to this mean-field theory varied widely, as discussed in (34).

The pairing gap of cold atoms and neutron matter are compared in the left panel of Fig. 2. At very low $k_F a$ the Gorkov-Melik-Barkhudarov analytic corrections to BCS theory are available (35). These corrections reduce the pairing gap by a factor of $1/(4e)^{1/3}$ from that obtained in the simple BCS theory, resulting in a pairing gap of:

$$\Delta^0(k_F) = \frac{1}{(4e)^{1/3}} \frac{8}{e^2} \frac{\hbar^2 k_F^2}{2m} \exp\left(\frac{\pi}{2ak_F}\right). \quad (6)$$

This pairing gap is, however, accurate only at small values of $k_F a$, and hence not applicable near the peak of the pairing gap.

At these larger values it is again useful to compare with the BCS-BEC transition in cold atom systems. In the extreme BEC limit, the BCS equation yields a pairing gap of 1/2 the binding energy of a pair, as the unpaired fermion can propagate nearly freely in the medium when the pairs are very strongly bound. There will be no further polarization corrections to this limit. It is natural to assume a smooth transition between the BCS limit, where the beyond-mean-field limits reduce the gap significantly, to the strongly-paired limit where the corrections are very small.

This smooth transition is in fact observed in cold atom experiments and in calculations of cold atoms and neutron matter. The pairing gap has been studied extensively experimentally, using both the density harmonically trapped up and down spins in a polarized system(6) and by studying the radio-frequency (RF) response (36). Analyses of the experimental result indicate a pairing gap of $0.45 \pm 0.05 E_F$, or approximately 65 per cent of the pairing gap found in the BCS theory.

The calculated pairing gaps in neutron matter are not as large as those in cold atoms because of the finite effective range. Eventually at larger momenta the s-wave interaction becomes repulsive. These higher order corrections result in a peak of the gap of about 0.3 times the Fermi energy at $k_F a \approx -5$, or $k_F \approx 0.25 - 0.3 \text{ fm}^{-1}$.

A variety of calculations of the pairing gap are shown in the right panel of Fig. 2. The simple BCS theory is shown as a solid line, other calculations include correlated-basis-function calculations (37, 38), polarization-potential (39), medium-polarization calculation (40), Brueckner (41), renormalization group (42),

determinantal lattice Monte Carlo calculations (43), Diffusion Monte Carlo (22), and AFDMC results (32, 44).

The pairing gaps do not agree nearly as well as the equation of state. However most of the approaches employed are not designed to handle the strong pairing that is present for neutron matter. Only the QMC approaches predicted the pairing gap in cold atoms and smoothly interpolate between BCS and BEC limits. They all result in rather large pairing gaps, with a modest reduction of the BCS result for pairing. The behavior of the pairing gap at higher densities is certainly interesting and important, particularly the p-wave gap, but requires additional study for a reliable prediction.

3 MODERATE DENSITIES: INTERACTIONS AND EQUATION OF STATE

Low-density neutron matter, as seen in the previous section, can be described by a neutron-neutron potential that is central, i.e. a function of the interparticle spacing alone, $V(r)$. As we saw, the essential features of the interaction can be captured by the s -wave scattering length a and the effective range r_e , i.e. only two numbers.

As the density increases different partial waves and spin-states come into the picture. That means that any formulation of the nucleon-nucleon potential needs to account for all of the allowed ways in which nucleons can interact with each other. Similarly, any quantum many-body method that is used to address interacting nucleons had better be able to handle the different partial waves and spin-states (and for the general case also isospin-states). In this section we first go over the basics of the operator structure of standard nuclear forces (both phenomenological ones and those following from chiral Effective Field Theory) before discussing results for the pure neutron matter equation-of-state (energy versus density) resulting from a variety of many-body methods.

3.1 Neutron-Neutron Interaction

Nucleon-nucleon (to be precise, np) scattering in different channels can be experimentally probed, so any nuclear force needs to reproduce a large number of scattering phase shifts. The different “channels” in which phase shifts are extracted from experiment are conveniently encapsulated in the spectroscopic notation $^{2S+1}L_J$: L denotes the orbital angular momentum using S, P, D, and so on. The $2S+1$ exponent for two neutrons can be either $2 \cdot 0 + 1 = 1$ (spin-singlet) or $2 \cdot 1 + 1 = 3$ (spin-triplet). Thus, the low-density s -wave scattering mentioned above which is dominant at low densities in neutron matter is given as 1S_0 . This is clearly seen in Fig. 3, which displays scattering phase shifts vs nucleon wave number/momentum: at vanishing momenta (corresponding to vanishing densities) the only phase shift that is non-zero is precisely the one in the 1S_0 channel. (the 3S_1 channel, familiar from the deuteron, does not come into play for the neutron-neutron case). We remind the reader that a positive phase shift corresponds to an attractive interaction: this implies that at very low densities the

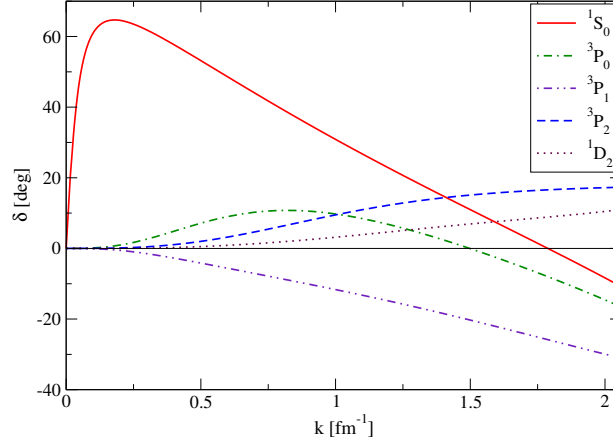


Figure 3: np scattering phase shifts vs the wave number of a nucleon in the center-of-mass frame (based on the Nijmegen93 partial-wave analysis). Charge-independence and charge-symmetry breaking terms would slightly change these results for the case of neutron-neutron scattering. Figure taken from (19).

interaction in the 1S_0 channel is attractive, turning repulsive at around $k = 1.7 \text{ fm}^{-1}$ (thereby retroactively explaining the gap closure we saw in the previous section). At higher densities/momenta, 3P_2 is clearly the dominant channel, leading to 3P_2 - 3F_2 pairing (the coupling being due to the tensor operator, see below).

Traditionally, the effective reproduction of phase shifts was accomplished via the breakup of the nucleon-nucleon potential in different channels, exemplified by the Argonne family of potentials (45). Here is the Argonne v8' (AV8') (23) case:

$$V_{12} = \sum_{p=1}^8 v^p(r) O_{12}^p, \quad (7)$$

Here O_{12}^p are spin-isospin dependent operators, which are given by:

$$O_{12}^{p=1,8} = (1, \boldsymbol{\sigma}_1 \cdot \boldsymbol{\sigma}_2, S_{12}, \mathbf{L} \cdot \mathbf{S}) \times (1, \boldsymbol{\tau}_1 \cdot \boldsymbol{\tau}_2). \quad (8)$$

In this expression $S_{12} = 3\boldsymbol{\sigma}_1 \cdot \hat{\mathbf{r}} \boldsymbol{\sigma}_2 \cdot \hat{\mathbf{r}} - \boldsymbol{\sigma}_1 \cdot \boldsymbol{\sigma}_2$ is the tensor operator, where $\mathbf{r} = \mathbf{r}_1 - \mathbf{r}_2$ is the nucleon separation vector. Similarly, $\mathbf{L} = -i\mathbf{r} \times (\nabla_1 - \nabla_2)$ is the relative angular momentum and $\mathbf{S} = \boldsymbol{\sigma}_1 + \boldsymbol{\sigma}_2$ is the total spin for the pair 12. An nn pair can only exist in an isotriplet state ($T = 1$), so $\boldsymbol{\tau}_1 \cdot \boldsymbol{\tau}_2 = 1$. The $v^p(r)$ functions in Eq. (7) contain one-pion exchange at large distances and high-quality phenomenology at intermediate and short distances.

More recently, the nuclear physics community has embraced chiral Effective Field Theory (EFT) interactions, in an attempt to connect with the symmetries of the underlying fundamental theory (Quantum Chromodynamics) (46, 47). In what follows, we provide a bare-bones description of chiral EFT, starting with the features that are common to all modern chiral EFT potentials. Chiral EFT interactions employ a separation of scales, that between pion and vector meson masses, and attempt to systematically expand in a small parameter that is the ratio between the two. Assuming the power counting employed is self-consistent,

this provides a hierarchy of forces controlled by the power of the expansion. Thus, chiral EFT systematically includes the analytically derived long-range one-pion exchange, as well as the intermediate-range two-pion exchanges, and so on. In addition to this, the power counting naturally leads to consistent three-nucleon and many-nucleon forces (e.g. at leading-order, LO, and next-to-leading order, NLO, no 3N forces are predicted). The soft scale, identified with the pion mass above, is generally taken to be that of a relevant momentum scale. In addition to the known pion exchanges, chiral EFT interactions also include phenomenological short-range terms, typically written down as Dirac-delta functions/contact terms: these do not reflect any deeper physics other than respecting all relevant symmetries and the power counting.

Before we look at specific expressions for the different parts of a chiral EFT interaction, we go over some definitions. Since chiral EFT interactions are based on a low-momentum expansion, it was natural that they were first formulated in momentum space. If we denote the incoming and outgoing relative momenta by $\mathbf{p} = (\mathbf{p}_1 - \mathbf{p}_2)/2$ and $\mathbf{p}' = (\mathbf{p}'_1 - \mathbf{p}'_2)/2$, respectively, then we can define the momentum transfer $\mathbf{q} = \mathbf{p}' - \mathbf{p}$ and the momentum transfer in the exchange channel $\mathbf{k} = (\mathbf{p}' + \mathbf{p})/2$. Generally speaking, terms that depend on \mathbf{q} are local and those depending on \mathbf{k} are non-local. The power expansion mentioned above is therefore an expansion in powers of \mathbf{q} and \mathbf{k} . Since our discussion is meant to be somewhat pedagogical, we limit ourselves below to the first three orders in the chiral expansion though, obviously, the pion exchanges and contact terms have also been extensively studied at higher orders.

Let us now look at the one- and two-pion exchanges in momentum space:

$$\begin{aligned} V_{1\pi,LO}^{\text{mom}} &= U_T(q) (\boldsymbol{\tau}_1 \cdot \boldsymbol{\tau}_2) (\boldsymbol{\sigma}_1 \cdot \mathbf{q}) (\boldsymbol{\sigma}_2 \cdot \mathbf{q}) \\ V_{2\pi,NLO}^{\text{mom}} &= W_C(q) (\boldsymbol{\tau}_1 \cdot \boldsymbol{\tau}_2) + V_S(q) (\boldsymbol{\sigma}_1 \cdot \boldsymbol{\sigma}_2) + V_T(q) (\boldsymbol{\sigma}_1 \cdot \mathbf{q}) (\boldsymbol{\sigma}_2 \cdot \mathbf{q}) \\ V_{2\pi,N^2LO}^{\text{mom}} &= V_C(q) + W_S(q) (\boldsymbol{\tau}_1 \cdot \boldsymbol{\tau}_2) (\boldsymbol{\sigma}_1 \cdot \boldsymbol{\sigma}_2) + W_T(q) (\boldsymbol{\tau}_1 \cdot \boldsymbol{\tau}_2) (\boldsymbol{\sigma}_1 \cdot \mathbf{q}) (\boldsymbol{\sigma}_2 \cdot \mathbf{q}) \end{aligned} \quad (9)$$

Note that all three of these expressions are functions of q alone (i.e. they are not functions of k). Thus, they can be trivially Fourier transformed and take the following form in coordinate space:

$$\begin{aligned} V_{1\pi,LO}^{\text{coord}} &= U_S(r) (\boldsymbol{\tau}_1 \cdot \boldsymbol{\tau}_2) (\boldsymbol{\sigma}_1 \cdot \boldsymbol{\sigma}_2) + U_T(r) (\boldsymbol{\tau}_1 \cdot \boldsymbol{\tau}_2) S_{12} \\ V_{2\pi,NLO}^{\text{coord}} &= W_C(r) (\boldsymbol{\tau}_1 \cdot \boldsymbol{\tau}_2) + V_S(r) (\boldsymbol{\sigma}_1 \cdot \boldsymbol{\sigma}_2) + V_T(r) S_{12} \\ V_{2\pi,N^2LO}^{\text{coord}} &= V_C(r) + W_S(r) (\boldsymbol{\tau}_1 \cdot \boldsymbol{\tau}_2) (\boldsymbol{\sigma}_1 \cdot \boldsymbol{\sigma}_2) + W_T(r) (\boldsymbol{\tau}_1 \cdot \boldsymbol{\tau}_2) S_{12} \end{aligned} \quad (10)$$

where we are only showing the finite-range parts of the pion exchange terms. It is easy to see, for example by focusing on the one-pion exchange term, that the $(\boldsymbol{\sigma}_1 \cdot \mathbf{q}) (\boldsymbol{\sigma}_2 \cdot \mathbf{q})$ term in momentum space gives rise to $\boldsymbol{\sigma}_1 \cdot \boldsymbol{\sigma}_2$ and S_{12} terms in coordinate space.

Note that the above expressions for the pion exchanges do not contain relativistic $1/m_N^2$ and $1/m_N$ corrections for the one- and two-pion exchange, respectively (where m_N is the nucleon mass). These would also involve (isoscalar and isovector) spin-orbit terms. This means that in chiral EFT the only spin-orbit term up

to order $N^2\text{LO}$ appears in the short-range contacts, which, as mentioned above, respect all relevant symmetries as well as the power counting. Qualitatively, working in momentum space, this means that at LO all 4 possible spin-isospin combinations should be present, without any momentum dependence. At NLO, something analogous holds: there are 14 different contact interactions that all contain a momentum-squared in some form. This can be summarized as:

$$\begin{aligned}
V_{\text{cont},LO}^{\text{mom}} &= \alpha_1 + \alpha_2 \boldsymbol{\sigma}_1 \cdot \boldsymbol{\sigma}_2 + \alpha_3 \boldsymbol{\tau}_1 \cdot \boldsymbol{\tau}_2 + \alpha_4 \boldsymbol{\sigma}_1 \cdot \boldsymbol{\sigma}_2 \boldsymbol{\tau}_1 \cdot \boldsymbol{\tau}_2 \\
V_{\text{cont},NLO}^{\text{mom}} &= \gamma_1 q^2 + \gamma_2 q^2 \boldsymbol{\sigma}_1 \cdot \boldsymbol{\sigma}_2 + \gamma_3 q^2 \boldsymbol{\tau}_1 \cdot \boldsymbol{\tau}_2 + \gamma_4 q^2 \boldsymbol{\sigma}_1 \cdot \boldsymbol{\sigma}_2 \boldsymbol{\tau}_1 \cdot \boldsymbol{\tau}_2 \\
&\quad + \gamma_5 k^2 + \gamma_6 k^2 \boldsymbol{\sigma}_1 \cdot \boldsymbol{\sigma}_2 + \gamma_7 k^2 \boldsymbol{\tau}_1 \cdot \boldsymbol{\tau}_2 + \gamma_8 k^2 \boldsymbol{\sigma}_1 \cdot \boldsymbol{\sigma}_2 \boldsymbol{\tau}_1 \cdot \boldsymbol{\tau}_2 \\
&\quad + \gamma_9 (\boldsymbol{\sigma}_1 + \boldsymbol{\sigma}_2)(\mathbf{q} \times \mathbf{k}) + \gamma_{10} (\boldsymbol{\sigma}_1 + \boldsymbol{\sigma}_2)(\mathbf{q} \times \mathbf{k}) \boldsymbol{\tau}_1 \cdot \boldsymbol{\tau}_2 \\
&\quad + \gamma_{11} (\boldsymbol{\sigma}_1 \cdot \mathbf{q})(\boldsymbol{\sigma}_2 \cdot \mathbf{q}) + \gamma_{12} (\boldsymbol{\sigma}_1 \cdot \mathbf{q})(\boldsymbol{\sigma}_2 \cdot \mathbf{q}) \boldsymbol{\tau}_1 \cdot \boldsymbol{\tau}_2 \\
&\quad + \gamma_{13} (\boldsymbol{\sigma}_1 \cdot \mathbf{k})(\boldsymbol{\sigma}_2 \cdot \mathbf{k}) + \gamma_{14} (\boldsymbol{\sigma}_1 \cdot \mathbf{k})(\boldsymbol{\sigma}_2 \cdot \mathbf{k}) \boldsymbol{\tau}_1 \cdot \boldsymbol{\tau}_2
\end{aligned} \tag{11}$$

(This is in momentum space, leading to a Dirac delta $\delta(r)$ in coordinate space, hence the name contacts.) It's obvious that this general set of contacts contains both q and k on an equal footing. In reality, only 2 and 7 of these contacts at LO and NLO, respectively, are linearly independent. As a rough mapping between momentum space and coordinate space, we note that the isoscalar spin-orbit term $(\boldsymbol{\sigma}_1 + \boldsymbol{\sigma}_2)(\mathbf{q} \times \mathbf{k})$ corresponds to $\mathbf{L} \cdot \mathbf{S}$.

All the chiral EFT terms mentioned above need to somehow be cut off (“regulated”) at high momenta in order to avoid infinities. Thus, they are multiplied with a regulator function:

$$f_\Lambda(p', p) = \exp \left[- \left(\frac{p'}{\Lambda} \right)^{2n} - \left(\frac{p}{\Lambda} \right)^{2n} \right] \tag{12}$$

where n is some power and Λ is known as the cutoff parameter, typically taken to be 400-500 MeV. This regulator and cutoff are used in the standard momentum-space formulations of chiral EFT by Entem-Machleidt (EM) (48) and Epelbaum-Glöckle-Meissner (EGM) (49). In addition to this, the EGM approach also uses a spectral-function regularization on the two-pion exchange terms given above (49), leading to a 2nd cutoff parameter, $\tilde{\Lambda}$ which is typically taken to be larger than Λ (700 MeV and above). It is also significant that nuclear forces with explicit Δ degrees of freedom are being investigated. (50,51)

More recently, two new chiral EFT potentials have appeared: i) $N^2\text{LO}_{\text{opt}}$ (52), which carried out a high-quality re-fit of the low-energy constants appearing in the contact terms, like those shown above, as well as the pion-nucleon couplings, and ii) local chiral EFT, (53,54) which made use of the afore-mentioned ambiguity in selecting the contacts such that they are quasi-local to begin with. [The latter approach also made use of a local regulator (i.e. one that is a function of q or r), as also adopted by a very recent mixed version of chiral EFT (55), which employs a local regulator and non-local contacts.] As will be seen in the many-neutron results discussed in the following subsection, the $N^2\text{LO}_{\text{opt}}$ potential is very soft, a feature which is useful to many-body methods that work in momentum space. On the other hand, the local chiral EFT approach has varied the cutoff Λ , producing a family of potentials, ranging from hard to quite soft.

3.2 Equation of State

While the nuclear force employed is an important component in describing neutron matter, just as important is the quantum many-body theory that is used to study the many-neutron problem. Details on specific results are given below, but let us first go over some general features of nuclear many-body methods. We limit our discussion to those methods that have been recently reformulated for (or applied to) neutron matter.

The first large distinction we could make is between *ab initio* methods, which try to solve the many-neutron Schrödinger equation employing varying degrees and types of approximations, and phenomenological approaches, which focus on reproducing and predicting experimentally relevant properties without necessarily seeking a connection to nuclear forces (56). *Ab initio* methods, in turn, can be grouped according to another general distinction, that between perturbative and non-perturbative methods. The prototypical perturbative method employed to describe neutron matter is Many-Body Perturbation Theory (MBPT), an approach which attempts to sum all classes of diagrams up to a specified order in interaction lines (57, 58, 59). On the other hand, non-perturbative nuclear methods can also be distinguished between a) resummation schemes, which sum a specific class of diagrams to all orders in the interaction, typically employing a ladder approximation, (60, 61), b) Coupled Cluster theory, which works by generating $np - nh$ excitations of a reference state, typically truncated at the doubles level (62), and c) Quantum Monte Carlo methods, in which the many-body problem is solved stochastically, (63, 33, 53, 64, 65). One could legitimately add to this list d) density functional theory, which *de facto* includes complicated many-body correlations and is applicable throughout the nuclear chart.

Given the significance of energy-density functional approaches of heavy nuclei, it is worthwhile to examine the interplay between *ab initio* calculations for neutron matter and EDF approaches. Ref. (66) explicitly showed that the equation-of-state (EOS) of neutron matter can be used to eliminate as unphysical several Skyrme energy-density functionals. As a result, the EOS of neutron matter has been, for a while now, used as a constraint in energy-density functional theories of nuclei (56). Recently, the interplay of Skyrme functionals and pure neutron systems was exploited in the context of the polaron/impurity problem (67), and more generally (68) – see also section 4 of the present review. The idea behind energy-density functional theories of nuclei is to use as input as much known physics as possible, in order to make predictions in regions where no experiment is possible (yet) and fully microscopic calculations are unrealistic. The use of microscopic results for pure neutron properties, then, ties in with that agenda, extending the input constraints beyond experiment: it stands to reason that neutron-rich nuclei predictions will depend critically on pure neutron constraints. Of course, the resulting EDFs can be applied to the context of neutron stars as well (69, 70), again addressing systems that are beyond the reach of *ab initio* approaches. Such density functionals could also explicitly include a neutron-star crust equation-of-state as input.

We now go over selected results on the equation of state of pure infinite neutron

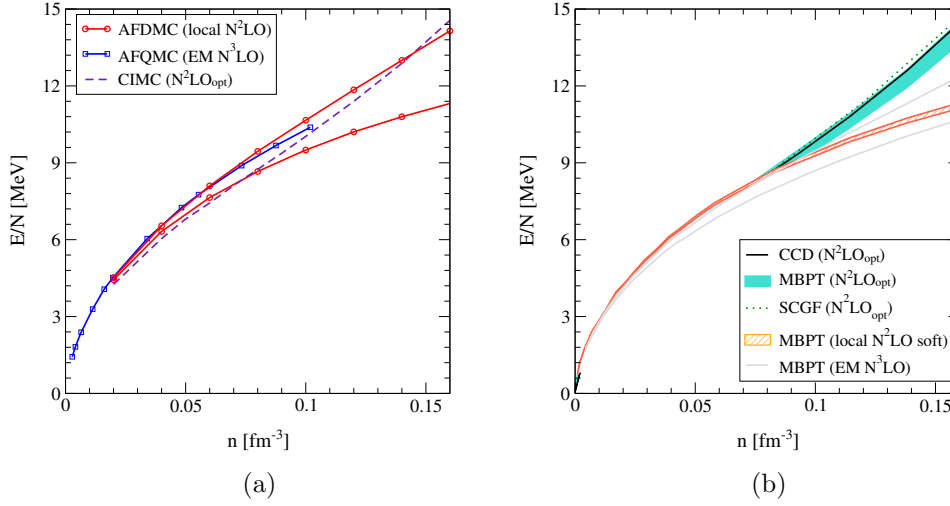


Figure 4: Equation-of-state of intermediate density neutron matter using only NN interactions as input. Shown are results for different chiral EFT potentials, different orders in the chiral expansion, and different quantum many-body methods. (a) Quantum Monte Carlo results, (b) All other many-body results. Details are provided in the main text.

matter, following from several quantum many-body approaches. All of these results use as input chiral EFT neutron-neutron interactions. It's important to note that if one is limited to the NN sector alone, the chiral EFT approach has no built-in advantage over phenomenological approaches like the Argonne family of potentials or CD-Bonn. One of the main distinguishing features of the chiral EFT approach is that it provides guidance (through its order-by-order expansion) on how to consistently pick the form of the 3N interaction. Thus, the results summarized in this subsection should be seen as the foundation of an approach that combines NN+3N forces, which become even more important at higher densities, as discussed later in this review.

We show in Fig. 4 results for the equation of state of neutron matter, following from calculations that use only nucleon-nucleon interactions as input. Specifically, we show MBPT results using local N²LO interactions as input (54) (specifically the soft 400 MeV potential), MBPT results using an N³LO EM potential (59), MBPT results using N²LO_{opt} (71), self-consistent Green's functions results using N²LO_{opt} (60), coupled-cluster doubles (CCD) results using N²LO_{opt} (62), AFDMC results using local N²LO interactions (54), Auxiliary-Field Quantum Monte Carlo (AFQMC) results using an N³LO EM potential (65), and configuration-interaction Monte Carlo (CIMC) results using N²LO_{opt} (64).

We see that at intermediate densities essentially all many-body methods with different input potentials give basically the same answer qualitatively (though that ceases to be the case closer to saturation density). At a more detailed level, within MBPT Fig. 4b seems to imply that as we go from N²LO to N³LO the energy decreases. Also, the MBPT plus soft local N²LO results are essentially

identical to the AFDMC plus soft local N^2LO ones (54). Intriguingly, the 414 MeV (soft) EM potential plus AFQMC of Ref. (65) leads to results that are similar to the 500 MeV (hard) local chiral potential plus AFDMC of Ref. (54). The MBPT results using N^2LO_{opt} of Ref. (71) underline how soft/perturbative the N^2LO_{opt} potential is: this implies that non-perturbative methods are not necessarily required to handle it. A distinguishing feature of the AFDMC results of (54) is the use of a fully non-perturbative QMC method to probe both soft and hard chiral potentials. Overall, it is clear from Fig. 4 that issues like the choice of different regulators and different cutoffs, as well as the non-locality vs locality of the potential employed, should be further investigated in detail. At vanishingly small densities the effects of pairing (discussed in an earlier section) would probably alter this picture, but such differences would likely not be visible at this scale.

3.3 Three Nucleon Interactions

It is well accepted that modern nucleon-nucleon interactions cannot describe the binding energies of nuclei with $A \geq 3$, and they have to be combined with three-body forces. In the framework of chiral EFT, as discussed in Sec. 3.1, the appearance of three- and higher many-body forces naturally emerges in the chiral expansion. However, in other approaches like for the Argonne interactions, the contribution of four-body forces is expected to be negligible. This observation comes from the fact that in nuclei and matter the three-body potential energy is (in magnitude) few percent than the two-body potential energy. The Urbana-IX (UIX) potential has been introduced to give a correct description of few-body systems. The UIX includes the Fujita–Miyazawa term that describes the p-wave exchange of two pions between three nucleons, where the intermediate state has one nucleon excited to a Δ , that is eventually integrated out. This term is the longest-range three-nucleon interaction and a very similar term also arises as the leading three-nucleon contribution (at N^2LO) in chiral perturbation theory (46). The Urbana models also include a spin-isospin independent short-distance term, that models the exchange of more pions between nucleons (72). The UIX force was originally proposed in combination with the Argonne AV18 and AV8' (73). It has been constructed to correctly describe the saturation of nuclear matter at $\rho_0 = 0.16 \text{ fm}^{-3}$, and to reproduce the binding energy of the 4He . Although this model of the three-nucleon force does not fully alleviate the underbinding problem in light nuclei, it has been extensively used to study the equation of state of nuclear and neutron matter (74, 33, 75, 76). It has to be noticed that the AV18+UIX Hamiltonian supported heavy mass neutron stars years before they have been observed.

Other phenomenological models of three-body force, such as the Illinois forces, have been obtained by fitting the binding energies of light nuclei up to $A \leq 8$ (77), and they give an excellent description of both ground- and excited-states of nuclei up to ${}^{12}C$ (78). In addition to the Fujita–Miyazawa term the Illinois models also include s-wave two-pion-exchange and also three-pion-exchange ring diagrams. Unfortunately, the three-pion rings included in the Illinois forces leads to a very

strong attraction in pure neutron-matter (79,80) at high densities, and produces EOS too soft to be compatible with observed neutron star masses and radii. This is a sign of important deficiencies in the model of the three-nucleon forces, which will become especially important at higher density and larger isospin asymmetry. Hamiltonians based on chiral EFT would be very valuable to address these issues. However, such interactions should be constructed to reproduce nucleon-nucleon scattering data up to large energies. A qualitative estimate is given by observing that the momentum of two neutrons is given by $k \approx \sqrt{E_{lab} m/2}$, and then if this is compared to the Fermi momentum of homogeneous matter we have $\rho \approx (E_{lab} m/2)^{3/2}/3\pi^2$ (of course, this is only a back-of-the-envelope calculation, so it does not account for possible prefactors). This clearly shows that if one wants to describe important correlations in neutron matter up to large densities, then a nucleon-nucleon interaction that accurately fitting phase-shifts up to large E_{lab} will be important. Of course, this raises the questions of which functional form for the three-nucleon force should be employed, as well as which observables the three-nucleon parameters should be fit to, when one interested in describing matter at high density.

4 INHOMOGENEOUS NEUTRON MATTER

The neutron matter in the exterior of neutron-rich nuclei or the inner crust of neutron stars is not homogeneous, so it is important to study the properties of neutron matter in confined geometries and with density gradients. Typically, nuclear density functionals have isoscalar and isovector gradient terms that allow for a different energy cost of density gradients between isospin symmetric nuclear matter and pure neutron matter. The isoscalar gradients can be very tightly constrained by the properties of finite nuclei, but the gradients in pure neutron matter are much less tightly constrained. To some degree this is a result of the fact that we have direct experimental extractions of the charge density through electron scattering, but less direct knowledge of the neutron density. At present there is a large extrapolation of experimental knowledge to the nearly pure neutron matter found between nuclei in the inner crust of neutron stars.

One avenue to extract additional information is to use microscopic theories of neutron matter in an external field. Different external fields can be used to probe different properties of neutron matter; to date finite systems have been studied using harmonic oscillator or Woods-Saxon external one-body potentials. These serve to confine the system and to constrain the densities. Originally these calculations were limited to very small systems (81), but more recently much larger systems have been treated where comparisons to density functionals are more meaningful (82).

Other properties of density functionals can also be studied in the pure neutron limit. The relative importance of pairing and shell gaps is tightly constrained by the measured properties of nuclei. Shell gaps in neutron matter are expected to be much smaller because of the strong pairing. Spin-orbit splitting can also be examined by studying systems away from closed shells.

4.1 Neutron Matter and Density Functionals

It is again instructive to compare results for confined systems in cold atoms with those in neutron matter. Cold atoms at unitarity have essentially no closed shells, as discussed below, and hence can be described as an expansion around the local density:

$$\mathcal{E}_2 = \int V_{ext}(r)\rho(r) + \xi \frac{3}{5}(3\pi^2)^{2/3}\rho^{5/3} + c_2 \nabla\rho^{1/2} \cdot \nabla\rho^{1/2} + c_4 \frac{\nabla^2\rho^{1/2}\nabla^2\rho^{1/2}}{\rho^{2/3}} + \dots, \quad (13)$$

where the first two terms provide the simple local-density approximation (LDA).

The form of this energy density functional is severely restricted by the scale-invariance of the cold atom system. All terms in the energy density must scale like $\rho^{5/3}$. Such a functional will not work for cold atoms at small $k_F a$ as in this BCS regime individual particles can propagate over the entire system and the fermionic closed shells are very important. While it is not obvious *a priori* that this simple density functional will work at unitarity, microscopic results using both Diffusion Monte Carlo and lattice Auxiliary Field Monte Carlo justify this simple local density plus gradient expansion form (83).

Clearly such a simple form will not work well for nuclei or neutron drops, where the fermionic shell closures play a critical role. Of course Skyrme and Hartree-Fock-Bogoliubov models play a critical role in the study of medium and heavy nuclei, including particularly neutron-rich nuclei (8). These density functionals have parameters that are fit to the properties of nuclei, and sometimes to the calculated bulk properties of neutron matter. A similar strategy should be helpful in constraining the gradient, spin-orbit, and pairing terms in very neutron-rich nuclei.

4.2 Neutron Drops

Here we summarize results for neutron drops in Harmonic Oscillator and Wood-Saxon external fields, and compare them to available results for cold atoms. A variety of different interactions and methods have been used for calculations of neutron drops (82, 84, 85, 86). In Fig. 5 we show results for neutrons trapped in a harmonic oscillator trap with a frequency of 10 MeV. Results for lower and higher trap frequencies have also been reported. For cold atoms lattice methods are used which are free of a sign problem; note that the cold atom results show essentially no evidence of the closed shells that would appear for non-interacting fermions with $N=8, 20, 40$, etc. The local density approximation with the bulk value of $\xi = 0.37$ for cold atoms is shown as a solid black line, finite drops rapidly and smoothly approach this bulk limit. Gradient corrections have been studied in Ref. (83). The dashed line indicates the local density approximation for $\xi = 0.50$, a value more appropriate for the neutron equation of state.

Calculations from 8 to 50 neutrons using the AV8' NN interaction and the AV8' + UIX NNN interaction are shown. The results plotted here use the AFDMC method; results for N up to 16 with GFMC are essentially identical. The three-nucleon interaction is not very important for small N , as the density is relatively

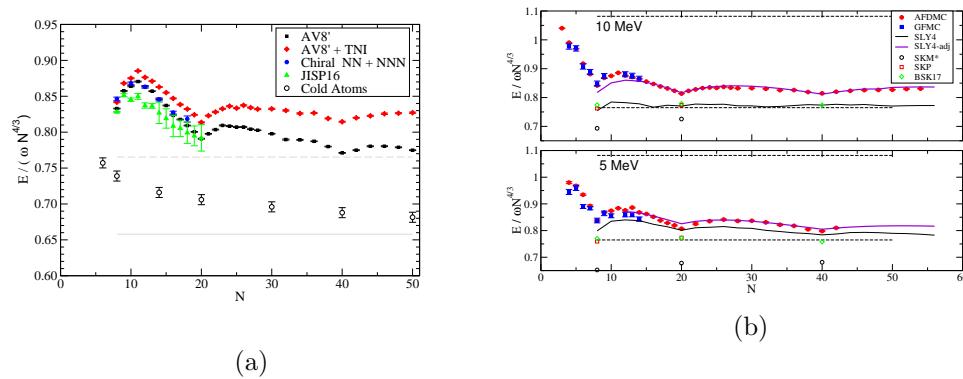


Figure 5: Energies for neutrons trapped in a harmonic oscillator with $\omega = 10$ MeV for different interactions and methods compared to Monte Carlo calculations for cold atoms at unitarity (open symbols) and two local density approximations (solid and dashed lines). In the right panel results for the AV8' + UIX interaction are compared to several pre-existing density functionals.

modest. For larger N , though, the central density in a harmonic trap can be quite large and the three-nucleon interaction makes a considerable difference. Results are also shown for no-core shell model (NCSM) calculations using chiral interactions and the JISP16 NN interaction. The chiral interactions are very similar to the AV8' results without a three-nucleon interaction; the energies for all interactions and methods agree within a few percent.

These calculations show significant shell closures, in contrast to the cold atom results. These shell closures arise because of the effective range in the neutron-neutron interaction, and the concomitant smaller size of the superfluid pairing gap. In cold atoms only superfluid pairs propagate across the whole system, while for neutrons the shell closures indicate the single-particle picture still survives to some degree. The shell closures are not as strong as in nuclei, however. Pairing gaps are also evident from the odd-even staggering, spin-orbit, and gradient corrections have been examined in many of these studies (84, 85).

In the right-hand panel, results for the AV8' + UIX interaction are compared with a variety of previously existing density functionals. These functionals do not fully describe the neutron drop results, in general their energy is too low and spin-orbit and pairing are not completely correct. Modest modifications to the isovector (full neutron) gradients, pairing and spin orbit give density functional results in the full black line, labeled SLY4+adj. These do a good job of reproducing results in both 5 and 10 MeV frequency traps except for the smallest systems considered. More recently it has been shown that new density functionals, i.e. UNEDF0 (87) and UNEDF1 (88), can be created that simultaneously fit nuclei with accuracy comparable or better than the existing functionals, and also reproduce the neutron drop results.

In figure 6 we show results in a Wood-Saxon well. These more nearly mimic

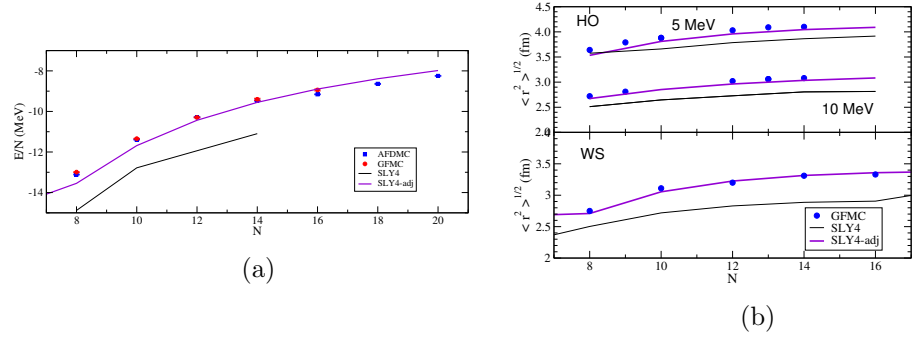


Figure 6: Energies for neutrons trapped in a Wood-Saxon external field compared with density functionals (left panel) and radii of neutron drops in HO and WS wells compared to density functionals (right panel).

nuclei since the central density is rather fixed, and hence they are not so sensitive to the high-density behavior of the equation of state. The same modified density functional that fits the harmonic oscillator results also reproduces the Wood-Saxon results, and simultaneously describes the calculated radii of drops in both external fields.

Further studies of inhomogeneous neutron matter are warranted, including effects of the three-nucleon interaction and different external fields. In the inner crust of a neutron star, for example, the neutrons are not small finite systems. Therefore it would be very useful to constrain the gradient terms with periodic external fields with a range of momenta, and see if the same density functional can describe these systems as well as finite drops.

5 HIGHER DENSITIES: NEUTRON MATTER AND NEUTRON STARS

At higher densities the three-nucleon interaction becomes even more important. These play an important role in the mass/radius relation for neutron stars. In this section we describe the equations of state obtained at higher densities including three-nucleon interaction results and the equation of state, describe the relation between the symmetry energy E_{sym} , the difference between neutron matter energy and isospin-symmetric nuclear matter energy at nuclear saturation density, and its density derivative L . Finally we describe the impact of these constraints on the neutron star mass-radius relation as well as describe briefly the importance of three-hadron neutron-neutron-lambda interactions in the equation of state of high-density neutron matter.

5.1 Equation of State

The EOS of neutron matter around nuclear densities is important for several reasons. As outlined in the previous sections, in this regime several channels contributing to the nucleon-nucleon interaction are important, and thus the EOS

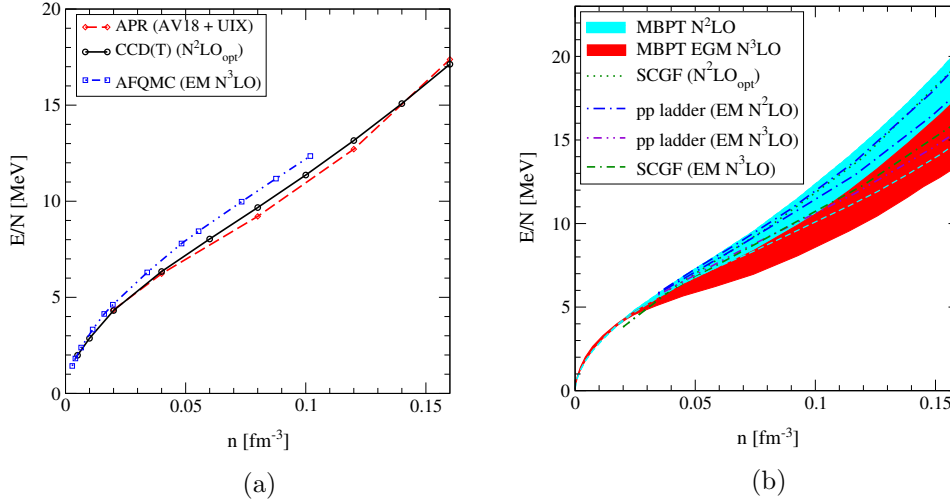


Figure 7: Equation-of-state of intermediate density neutron matter using both NN interactions and 3NF as input. Shown are results for different chiral EFT potentials, different orders in the chiral expansion, and different quantum many-body methods. (a) The standard APR results, along with Coupled Cluster and Auxiliary-Field Quantum Monte Carlo results (b) Many-body perturbation theory, Self-Consistent Green's Function, and pp ladder approximation results. Details on the interactions employed are given in the main text.

provides a direct comparison between different frameworks for the nuclear Hamiltonian. Although the maximum mass of neutron stars is dominated by the EOS at very high densities, their radius is determined by the pressure in the region of about 1 to 2 ρ_0 , and then measurements of radii of neutron stars can be used to constrain the EOS.

We show in Fig. 7 results for the equation of state of neutron matter at somewhat smaller densities, following from calculations that use both nucleon-nucleon and three-nucleon interactions as input. Specifically, we show MBPT results using EM and EGM N^2LO interactions as input (the lower end of this band is shown using a dashed line), (58) MBPT results using N^3LO EM potentials, (58) results following from a particle-particle ladder approximation using N^2LO EM potentials, (61) as well as pp ladder results using an N^2LO EM potential, (61) self-consistent Green's functions (SCGF) results using $\text{N}^2\text{LO}_{\text{opt}}$, (60) as well as SCGF results using EM N^3LO as input, (60) Coupled-Cluster with doubles and including some triples effects, CCD(T), results using the $\text{N}^2\text{LO}_{\text{opt}}$ interaction, (62) Auxiliary-Field Quantum Monte Carlo (AFQMC) results using an N^3LO EM potential, (65) as well as the frequently cited Akmal-Pandharipande-Ravenhall results using AV18 plus UIX (74).

The most obvious feature of Fig. 7 in comparison to Fig. 4 is that three-nucleon interactions in neutron matter are repulsive, i.e. the energy goes up: this is in contradistinction with what holds in light and medium-mass nuclei. Another general aspect of this figure relates to the transition from N^2LO to N^3LO : in

Fig. 7b for MBPT, SCGF and the pp ladder approximation results are shown for both orders in the chiral expansion, and in both cases the energy decreases. This is despite the fact that the MBPT results use consistent interactions, i.e. include an $N^3\text{LO}$ 3N force along with the $N^3\text{LO}$ NN force, while the pp ladder and SCGF values, like most other many-body results currently available, combine the $N^3\text{LO}$ NN force with $N^2\text{LO}$ at the 3N level. Also prominent is the fact that the SCGF $N^2\text{LO}_{\text{opt}}$ results reasonably match the EM $N^2\text{LO}$ pp ladder values (and similarly for the corresponding EM $N^3\text{LO}$ ones), which is probably not unexpected (with the exception of the low-density region). A final noteworthy feature is that the CCD(T) results appear to match rather nicely with the APR values. A conclusion that the Figs. 4 & 7 really underline is the significance of producing error bands using more than one potential as input, if possible employing a non-perturbative or otherwise controlled approximation scheme.

Around density ρ_0 , the EOS of pure neutron matter is directly related to the symmetry energy and its slope, and the analogous (and much more challenging) calculation of symmetric nuclear matter is not needed. The symmetry energy $E_{\text{sym}}(\rho)$ is generally defined as the difference between the energy of pure neutron matter and the energy of symmetric nuclear matter with the same total baryon density. In terms of the isospin asymmetry, $x \equiv \rho_p/\rho$, the energy per nucleon of isospin asymmetric nuclear matter is commonly expanded in even powers of x ,

$$E(\rho, x) = E_0(\rho) + E_{\text{sym}}^{(2)}(\rho)(1 - 2x)^2 + E_{\text{sym}}^{(4)}(\rho)(1 - 2x)^4 + \dots, \quad (14)$$

where E is the energy per nucleon of the system, $E_0(\rho) = E(\rho, x = 0.5)$ is the EOS of symmetric nuclear matter, and $E_{\text{sym}}^{(4)}(\rho)$ and higher order corrections are ignored here. The symmetry energy E_{sym} is then given by

$$E_{\text{sym}}(\rho) = E(\rho, 0) - E_0(\rho), \quad (15)$$

where $E(\rho, 0)$ is the EOS of pure neutron matter. Near the nuclear saturation density, ρ_0 , there are a number of constraints on the EOS of infinite nuclear matter from nuclear masses, charge radii, and giant resonances. The extrapolation of the binding energy of heavy nuclei to the thermodynamic limit yields $E_0(\rho_0) = -16.0 \pm 0.1$ MeV (89). Because the pressure is zero at saturation, the symmetry energy can be expanded around saturation as

$$E_{\text{sym}}(\rho) \Big|_{\rho_0} = E_{\text{sym}} + \frac{L}{3} \frac{\rho - \rho_0}{\rho_0} + \dots, \quad (16)$$

where E_{sym} is the symmetry energy at saturation, and L is a parameter related to its slope. It is convenient to first focus to E_{sym} at ρ_0 for several reasons. The calculation of symmetric nuclear matter is much more challenging than pure neutron matter, mainly because the Hamiltonian is more complicated, and isospin symmetric matter is more strongly correlated through the tensor interaction acting in S - and D -waves. In particular, in the low density regions clustering effects are very difficult to be included in the calculation of the EOS, and/or isolated from experimental measurements.

Using QMC methods, the EOS of pure neutron matter is typically calculated with a simulation of 66 particles in a box imposing periodic boundary conditions, for which finite size effects are generally very well under control (79,33). A comprehensive study of the model of the three-neutron interaction has been presented in Ref. (75), with particular emphases to the role played by short range correlations. Within the Urbana/Illinois models, the main contribution of the three-body force is given by the short-range part, whose structure in the UIX model is

$$V_{ijk}^R = A_R \sum_{\text{cyc}} T^2(m_\pi r_{ij}) T^2(m_\pi r_{jk}), \quad (17)$$

where m_π is the pion mass, and

$$T(x) = \left(1 + \frac{3}{x} + \frac{3}{x^2}\right) \frac{e^{-x}}{x} \xi^2(x). \quad (18)$$

The function $\xi(x) = 1 - e^{-cx^2}$ is a cutoff function to regularize $T(x)$ at small distances. The V^R term basically models the four-pion exchange between neutrons (90). In order to address the role of the above short-distance behavior, other forms for V_{ijk}^R have been considered, in addition to different models of intermediate- and long-range contributions of the three-body force. These terms, where two or three pions are exchanged between neutrons, with the creation of Δ excited states, are described in Ref. (77).

The resulting EOS are shown in Fig. 8, where we compare the results obtained with the AV8' and AV8'+UIX Hamiltonians with several EOS obtained using different models of three-neutron interactions, adjusted to give the value for E_{sym} indicated in the figure. The range of E_{sym} is compatible with several experimental measurements (91,92). To obtain a lower symmetry energy with the AV8' model of two-body force would require an attractive contribution of the three-body force. The three-pion rings give attraction in pure neutron matter (80), but they would require a strong short-range repulsion to make the EOS stiff enough to support astrophysical observations.

The EOS calculated using QMC can be conveniently parametrized using the following functional form:

$$E(\rho_n) = a \left(\frac{\rho_n}{\rho_0}\right)^\alpha + b \left(\frac{\rho_n}{\rho_0}\right)^\beta, \quad (19)$$

where $E(\rho_n)$ is the energy per neutron as a function of the neutron density ρ_n , and the parameters a , α , b , and β are obtained by fitting the QMC results. The parametrization of the equations of state obtained with the AV8' and AV8'+UIX Hamiltonians are reported in (93).

Using Eq. (16) the value of E_{sym} and L can be easily extracted from the calculated EOS. The result are shown in Fig. 9, where we compare the results obtained using the AV8' and AV8'+UIX Hamiltonians (red and black symbols), the various EOS giving the indicated E_{sym} obtained by changing the three-neutron force model (green and blue symbols), and results obtained using the Illinois model of three-neutron force that includes three-pion rings where we have independently

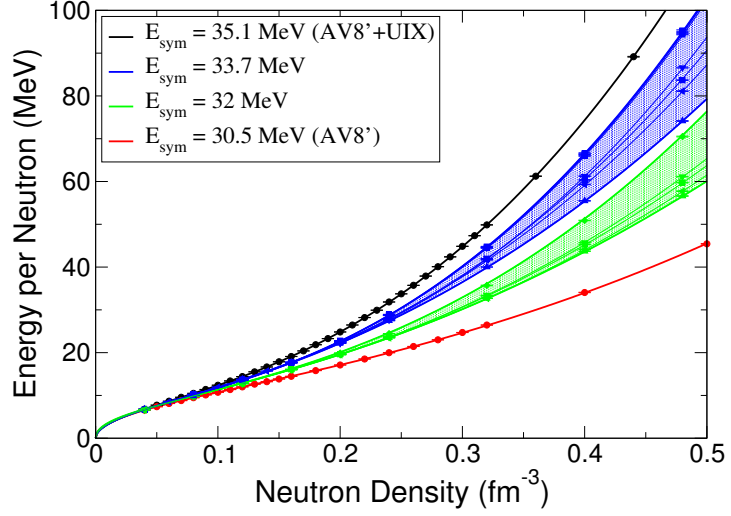


Figure 8: The equation of state of neutron matter obtained by using various models of three-neutron force as described in the text. For each model we impose that the energy at saturation is 17.7(1) MeV (blue band), or 16.0(1) MeV (green band). The results are compared with the equations of state obtained with the AV8' and AV8'+UIX Hamiltonians. In the legend we indicate the corresponding symmetry energy at saturation. Figure taken from (93).

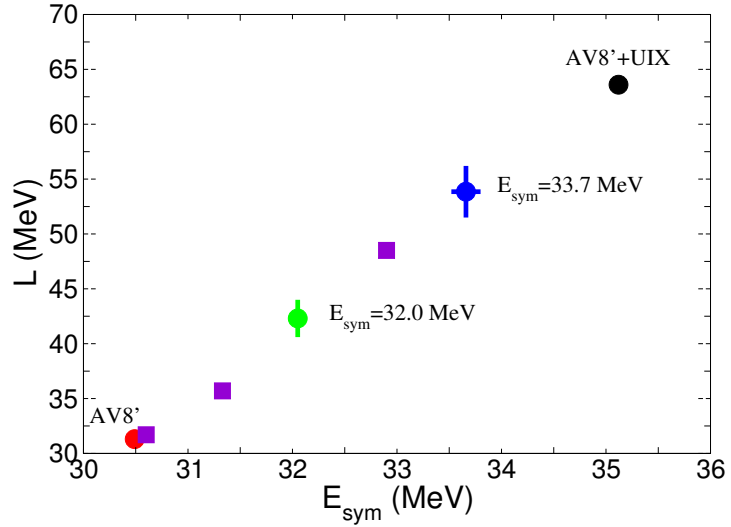


Figure 9: The value of L as a function of E_{sym} obtained from various EOS. The green and blue points with error bars correspond to the various EOS indicated by the two colored areas of Fig. 8, and red and black points show the results obtained using a two-body force alone and combined with the UIX model. The square symbols correspond to results obtained by independently changing the cutoff parameters entering in V_R and in the three-pion rings of the three-neutron force. Figure taken from (93).

changed the cutoff of the intermediate- and short-range part. It is clear that within this model the correlation between L and E_{sym} is very strong.

5.2 Neutron Star Mass/Radius

The neutron star matter is mainly composed by neutrons and a few protons. When the EOS of the neutron-star matter has been specified, the structure of an idealized spherically-symmetric neutron star model can be calculated by integrating the Tolman-Oppenheimer-Volkoff (TOV) equations:

$$\frac{dP}{dr} = -\frac{G[m(r) + 4\pi r^3 P/c^2][\epsilon + P/c^2]}{r[r - 2Gm(r)/c^2]}, \quad \frac{dm(r)}{dr} = 4\pi r^2 \epsilon, \quad (20)$$

where $m(r)$ is the gravitational mass enclosed within a radius r , and G is the gravitational constant. The above equations are solved by obtaining the energy density ϵ and pressure P from the EOS, and by specifying an initial point in the integration that is given by the central density of the star. For the EOS with the form of Eq. 19 we have

$$\epsilon = \rho_0 \left[a \left(\frac{\rho}{\rho_0} \right)^{1+\alpha} + b \left(\frac{\rho}{\rho_0} \right)^{1+\beta} + m_n \left(\frac{\rho}{\rho_0} \right) \right], \quad (21)$$

and

$$P = \rho_0 \left[a\alpha \left(\frac{\rho}{\rho_0} \right)^{1+\alpha} + b\beta \left(\frac{\rho}{\rho_0} \right)^{1+\beta} \right]. \quad (22)$$

The solution of the TOV equations gives, for a specified central density ρ_c , the profiles of ρ , ϵ and P as functions of radius r , and also the total radius R and mass $M = m(R)$. The total radius R is defined to the point where the pressure vanishes. The solution of the TOV equations are modified only slightly by magnetic fields and temperatures which are expected, and rotation is less than a 10% effect for the kinds of M-R curves which we present below. The speed of sound, c_s in the neutron star interior is $c_s^2 = dP/d\epsilon$, and ensuring that this is less than the speed of light (and thus the EOS is said to be “causal”) constrains the set of possible EOS. Also, the pressure must increase with increasing energy density, $dP/d\epsilon > 0$, in order to ensure that the neutron star is hydrodynamically stable.

In practice, the crust of neutron stars cannot be modeled with a pure neutron matter EOS. Several approaches to describing the EOS of neutron-star matter exist, including the combination of microscopic calculations based on chiral EFT with polytropes put forward in (94,95). All the results presented in this section have been obtained by using QMC calculations shown in the above sections for densities $\rho \geq \rho_{\text{crust}} = 0.08 \text{ fm}^{-3}$. At lower densities the neutron star matter is modeled by using the EOS of the crust obtained in Refs. (96,97). When the EOS violates causality (this is very often the case of EOS obtained from non-relativistic nuclear Hamiltonians), the EOS is switched to the maximally stiff EOS. The TOV equations are solved for several values of ρ_c , and the solution giving the maximum mass is considered.

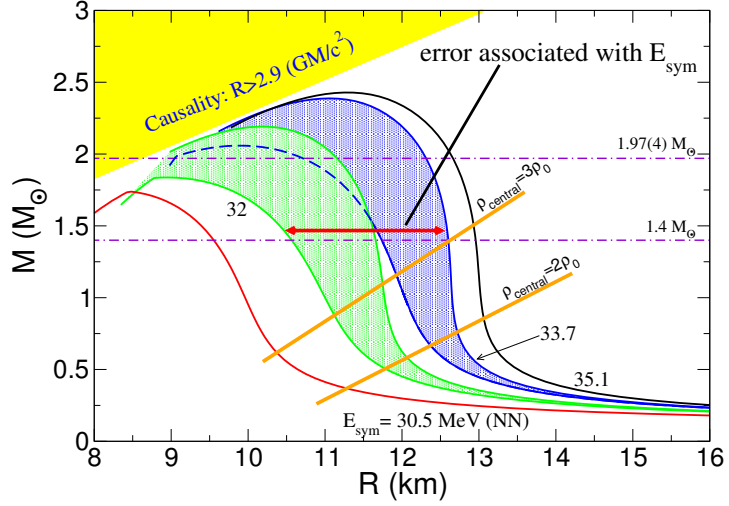


Figure 10: The mass-radius relation for neutron stars based on the QMC neutron matter results above. Results are presented for the different EOS given in Fig. 8. The numbers indicate the value of E_{sym} of the various EOS.

By using the EOS obtained from different nuclear Hamiltonian, we can study the effect to the neutron star structure. The results of the M-R diagram of neutron stars obtained from the EOS calculated in the previous section are shown in Fig. 10. Since the radii of neutron stars are almost determined by the EOS slightly above ρ_0 (98), future measurements will provide strong constraints to the nuclear Hamiltonian. In particular, radii are directly connected to the pressure of neutron matter at ρ_0 , and then there is a natural correlation between E_{sym} and L and radii. In the figure the two bands correspond to the EOS described in the previous section (the corresponding values of the symmetry energy are also indicated in the figure). The red and black curves correspond to the EOS calculated with the AV8' two-body interaction alone, and combined with the UIX three-neutron potential. The relation between E_{sym} and the radius is evident, as the increasing of E_{sym} predicts a neutron star with a larger radius. In the figure, the density of the neutron matter inside the star is indicated with the orange lines. As anticipated, even at large masses the radius of the neutron star is mainly governed by the equation of state of neutron matter between 1 and 2 ρ_0 (98).

As is clear from the figure, the AV8' Hamiltonian alone does not support the recent observed neutron star with a mass of $1.97(4)M_\odot$ (9) and $2.01(4)M_\odot$ (10). the addition of a three-body force to AV8' can provide sufficient repulsion to be consistent with all of the constraints. The results also suggest that the most modern neutron matter EOS imply a maximum neutron star radius not larger than 13.5 km, unless a drastic repulsion sets in just above the saturation density (75). This rules out EOS with large values of L , typical of Walecka-type mean-field models without higher-order meson couplings which can decrease L . We note that our analysis suggests it is unlikely that neutron stars have radii lower than

10 km (13,14), and/or larger than 15 km, but determining the systematic uncertainties is still an open question (99).

These recent observations of neutron stars with $1.97(4)M_{\odot}$ (9) and $2.01(4)M_{\odot}$ (10) put the most severe constraints on the EOS, although the precise hadronic composition is still undetermined. When the EOS is stiff, the corresponding chemical potential is large enough that heavier particles, hyperons, can be created from neutrons. For example, in the case of neutrons the Λ particles might form, and a fundamental question is about their role to the EOS. Note that other lighter hyperons (like Σ) would form at higher densities because they need that the proton fraction is large enough, and consequently their production is suppressed compared to Λ . The main uncertainty in the inclusion of hyperons is because the nucleon-hyperon (and the hyperon-hyperon) interaction is not well understood. For example, several calculations based on Brueckner-Hartree-Fock suggest that when hyperons are included in the EOS, the corresponding mass of neutron stars is very low (100). Other calculations based on relativistic mean-field or similar methods instead do not exclude that the inclusion of hyperons give neutron stars that are not compatible with recent observations. The Λ -nucleon potential, and in particular the importance of the Λ -neutron-neutron interaction, has been recently discussed by comparing QMC calculations of the binding energy of hypernuclei with available experimental measurements (101,102). The role of Λ hyperons in neutron star matter has been discussed by Lonardoni et al. in Ref. (103). The main conclusion is that a small change of the Λ -neutron-neutron interaction, while producing very small changes to the properties of hypernuclei, has a dramatic effect in neutron matter.

In Fig. 11 we show the mass-radius of neutron stars obtained by including the Λ hyperons to the EOS. As described in Ref. (103), the fraction of Λ is determined by imposing chemical equilibrium once the energy as a function of the concentrations of Λ is known. That has been calculated using the AFDMC method for different Hamiltonians. The AV8'+UIX for the pure neutron sector has been combined with the Λ -nucleon interaction of Ref. (104), and with the addition of two different Λ -nucleon-nucleon potentials, denoted as $\Lambda N + \Lambda NN$ (I) and $\Lambda N + \Lambda NN$ (II). While the operatorial structure of these forces is the same, the strengths have been slightly changed to reproduce better the binding energy of Λ -hypernuclei. Although the two Hamiltonians give qualitatively very similar results in hypernuclei, the EOS and the corresponding neutron star structure are dramatically different. It is clear that further input on hyperon-nucleon interactions, especially on ΛNN , will be crucial if firm conclusions are to be drawn.

6 CONCLUSIONS AND OUTLOOK

A great deal has been learned about neutron matter over the past decade, both from theory and through experiments and observations. The equation of state of cold neutron matter at low and moderate densities is now tightly constrained from many-body calculations with realistic interactions. Also, the pairing gap has been reliably extracted from methods that correctly predicted the pairing

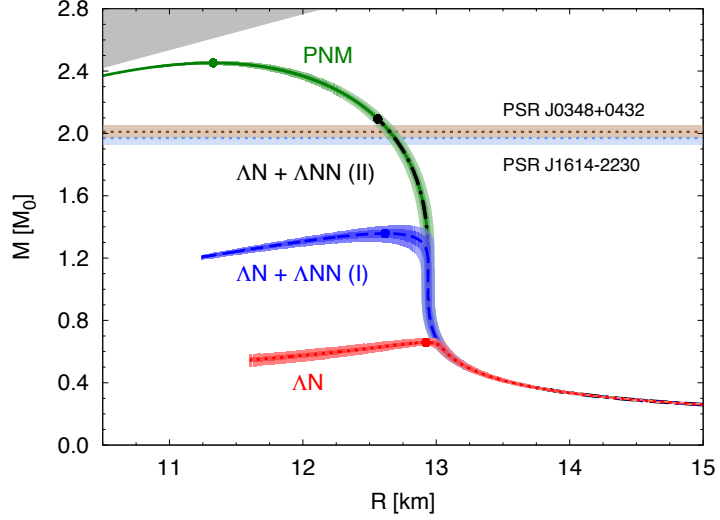


Figure 11: The mass-radius for neutron stars obtained from EOS that include Λ -hyperons. The green upper line (denoted with PNM) is the result of pure neutron matter (the same presented in Fig. 10). The red bottom band (indicated with ΛN) is obtained by including only the Λ -nucleon interaction in the Hamiltonian. The blue curve, $\Lambda N + ANN$ (I), is obtained but including the Usmani three-body interaction (104). The EOS obtained using the $\Lambda N + ANN$ (II) does not allow to Λ hyperons to produce, and is indicated by the dashed black line. Recent heavy-mass neutron stars measurements are also indicated by horizontal lines. Figure taken from (103).

gap in Fermi atoms at unitarity, a similarly strongly paired Fermi system.

Calculations of the equation of state provide strong constraints on the radii of typical neutron stars of masses ≈ 1.4 solar masses. These seem to be in reasonable agreement with mass/radius constraints extracted from astrophysical observations, but the observations and particularly the associated extraction of the mass/radius relation remain a controversial area with a variety of results.

Constraints on inhomogeneous matter are also starting to appear: it is encouraging that these results can be made consistent with density functionals that also describe nuclei. Traditionally, density functionals have used limited constraints at the extremes of isospin, so this remains a promising avenue for future research. It will be interesting to see if these constraints alter predictions for the properties of neutron-star crusts.

Finally, the observation of two-solar-mass neutron stars has challenged the traditional view that hyperons and other non-nucleonic degrees of freedom will appear and considerably soften the high-density equation of state. In the case of hyperons, the role of the hyperon-two-nucleon interaction is very important, and may limit the role of hyperons in dense neutron-rich matter. Studies of cold dense matter from the fundamental degrees of freedom, quarks and gluons, remain critical, though they are quite challenging.

There are many prospects for important further advances, both in theory and in experiments and observations. Experiments at rare isotope facilities will allow us to study many important neutron-rich nuclei, providing valuable information on neutron-rich matter. Observations and improved understanding should enable better constraints on the neutron-star mass-radius relation. The observation of gravitational waves associated with neutron-star mergers is an exciting possibility, and this could provide important constraints on neutron-star properties in the near future.

Our increasing ability to calculate properties of strongly interacting quantum systems will also play an important role. Neutron-star matter typically contains approximately ten percent protons: the impact on the neutron star mass/radius relation is likely to be modest but it may be very important for dynamic properties including the weak response of dense neutron matter. The role of superfluidity at higher densities, both p-wave superfluidity in neutrons and s-wave superfluidity of the low-density protons, is another important problem. Finally, studies of matter at finite temperature are critical for both potential sites of heavy-element synthesis, core-collapse supernovae, and neutron-star mergers.

DISCLOSURE STATEMENT

The authors are not aware of any affiliations, memberships, funding, or financial holdings that might be perceived as affecting the objectivity of this review.

ACKNOWLEDGMENTS

We would like to acknowledge valuable discussions with A. Carbone, E. Epelbaum, G. Hagen, K. Hebeler, J. W. Holt, T. Krüger, A. Lovato, D. Lonardoni, S. Pieper, S. Reddy, R. Sharma, K. Schmidt, A. Schwenk, I. Tews, R. Wiringa, G. Wlazlowski. The work of S.G. and J.C. was supported by the U.S. Department of Energy, Office of Nuclear Physics, under contract DE-AC02-05CH12231, and by the NUCLEI SciDAC project. The work of A.G. was supported by the Natural Sciences and Engineering Research Council of Canada. This work was accomplished with generous computer support provided by the INCITE program, Argonne and Los Alamos National Labs, NERSC, and the Jülich Supercomputing Center.

LITERATURE CITED

1. Giorgini S, Pitaevskii LP, Stringari S. *Reviews of Modern Physics* 80:1215 (2008)
2. Ku MJH, Sommer AT, Cheuk LW, Zwierlein MW. *Science* 335:563 (2012)
3. Carlson J, Gandolfi S, Schmidt KE, Zhang S. *Phys. Rev. A* 84:061602 (2011)
4. Schirotzek A, Shin YI, Schunck CH, Ketterle W. *Physical Review Letters* 101:140403 (2008)
5. Carlson J, Reddy S. *Physical Review Letters* 95:060401 (2005)

6. Carlson J, Reddy S. *Physical Review Letters* 100:150403 (2008)
7. Balantekin AB, et al. *Modern Physics Letters A* 29:30010 (2014)
8. Bender M, Heenen PH, Reinhard PG. *Reviews of Modern Physics* 75:121 (2003)
9. Demorest PB, et al. *Nature* 467:1081 (2010)
10. Antoniadis J, et al. *Science* 340:448 (2013)
11. Steiner AW, Lattimer JM, Brown EF. *The Astrophysical Journal Letters* 765:L5 (2013)
12. Steiner AW, Gandolfi S. *Phys. Rev. Lett.* 108:081102 (2012)
13. Özel F, Baym G, Güver T. *Phys. Rev. D* 82:101301 (2010)
14. Guillot S, Servillat M, Webb NA, Rutledge RE. *The Astrophysical Journal* 772:7 (2013)
15. Bauswein A, Janka HT. *Physical review letters* 108:011101 (2012)
16. Howell C, et al. *Physics Letters B* 444:252 (1998)
17. González Trotter DE, et al. *Physical Review Letters* 83:3788 (1999)
18. Bertsch GF. <http://www.phys.washington.edu/~mbx/george.html> (1998)
19. Gezerlis A, Pethick CJ, Schwenk A arXiv:1406.6109 [nucl-th] (2014)
20. Gezerlis A, Carlson J. *Phys. Rev. C* 77:032801 (2008)
21. Carlson J, Gandolfi S, Gezerlis A. *Progress of Theoretical and Experimental Physics* 2012:01A209
22. Gezerlis A, Carlson J. *Phys. Rev. C* 81:025803 (2010)
23. Wiringa RB, Pieper SC. *Phys. Rev. Lett.* 89:182501 (2002)
24. Lenz W. *Z. Phys.* 56:778 (1929)
25. Lee TD, Yang CN. *Phy. Rev.* 105:1119 (1957)
26. Forbes MM, Gandolfi S, Gezerlis A. *Phys. Rev. Lett.* 106:235303 (2011)
27. Friedman B, Pandharipande V. *Nuclear Physics A* 361:502 (1981)
28. Akmal A, Pandharipande V, Ravenhall D. *Physical Review C* 58:1804 (1998)
29. Baldo M, Maieron C. *Phys. Rev. C* 77:015801 (2008)
30. Schwenk A, Pethick CJ. *Phys. Rev. Lett.* 95:160401 (2005)
31. Carlson J, Morales J, Pandharipande V, Ravenhall D. *Phys. Rev. C* 68:025802 (2003)
32. Gandolfi S, et al. *Phys. Rev. Lett.* 101:132501 (2008)
33. Gandolfi S, et al. *Phys. Rev. C* 79:054005 (2009)
34. Dean DJ, Hjorth-Jensen M. *Rev. Mod. Phys.* 75:607 (2003)
35. Gorkov LP, Melik-Barkudarov TK. *JETP* 40:1452 (1961)
36. Shin YI, Schunck CH, Schirotzek A, Ketterle W. *Nature* 451:689 (2008)
37. Chen J, Clark J, Davé R, Khodel V. *Nuclear Physics A* 555:59 (1993)
38. Fabrocini A, Fantoni S, Illarionov AY, Schmidt KE. *Physical review letters* 95:192501 (2005)
39. Wambach J, Ainsworth T, Pines D. *Nuclear Physics A* 555:128 (1993)
40. Schulze HJ, et al. *Physics Letters B* 375:1 (1996)
41. Cao L, Lombardo U, Schuck P. *Physical Review C* 74:064301 (2006)
42. Schwenk A, Friman B, Brown GE. *Nuclear Physics A* 713:191 (2003)
43. Abe T, Seki R. *Physical Review C* 79:054003 (2009)
44. Gandolfi S, et al. *Phys. Rev. C* 80:045802 (2009)

45. Wiringa RB, Stoks VGJ, Schiavilla R. *Phys. Rev. C* 51:38 (1995)
46. Epelbaum E, Hammer HW, Meißner UG. *Rev. Mod. Phys.* 81:1773 (2009)
47. Machleidt R, Entem DR. *Phys. Rep.* 503:1 (2011)
48. Entem DR, Machleidt R. *Phys. Rev. C* 68:041001 (2003)
49. Epelbaum E, Glöckle W, Meiner UG. *The European Physical Journal A - Hadrons and Nuclei* 19:125 (2004)
50. Krebs H, Epelbaum E, Meissner UG. *The European Physical Journal A* 32:127 (2007)
51. Piarulli et al. M arXiv:1412.6446 [nucl-th] (2014)
52. Ekström A, et al. *Phys. Rev. Lett.* 110:192502 (2013)
53. Gezerlis A, et al. *Phys. Rev. Lett.* 111:032501 (2013)
54. Gezerlis A, et al. *Phys. Rev. C* 90:054323 (2014)
55. Epelbaum E, Krebs H, Meissner UG arXiv:1412.0142 [nucl-th] (2014)
56. Bender M, Heenen PH, Reinhard PG. *Rev. Mod. Phys.* 75:121 (2003)
57. Hebeler K, Schwenk A. *Phys. Rev. C* 82:014314 (2010)
58. Tews I, Krüger T, Hebeler K, Schwenk A. *Phys. Rev. Lett.* 110:032504 (2013)
59. Coraggio L, et al. *Phys. Rev. C* 87:014322 (2013)
60. Carbone A, Rios A, Polls A. *Phys. Rev. C* 90:054322 (2014)
61. Sammarruca F, et al. arXiv:1411.0136 [nucl-th] (2014)
62. Hagen G, et al. *Phys. Rev. C* 89:014319 (2014)
63. Schmidt KE, Fantoni S. *Phys. Lett. B* 446:99 (1999)
64. Roggero A, Mukherjee A, Pederiva F. *Phys. Rev. Lett.* 112:221103 (2014)
65. Wlazłowski G, et al. *Phys. Rev. Lett.* 113:182503 (2014)
66. Alex Brown B. *Phys. Rev. Lett.* 85:5296 (2000)
67. Forbes MM, et al. *Phys. Rev. C* 89:041301 (2014)
68. Brown BA, Schwenk A. *Phys. Rev. C* 89:011307 (2014)
69. Dutra M, et al. *Phys. Rev. C* 85:035201 (2012)
70. Erler J, et al. *Phys. Rev. C* 87:044320 (2013)
71. Tews I, et al. arXiv:1310.3643 [nucl-th] (2013)
72. Carlson J, Pandharipande VR. *Nucl. Phys. A* 371:301 (1981)
73. Pudliner BS, Pandharipande VR, Carlson J, Wiringa RB. *Phys. Rev. Lett.* 74:4396 (1995)
74. Akmal A, Pandharipande VR, Ravenhall DG. *Phys. Rev. C* 58:1804 (1998)
75. Gandolfi S, Carlson J, Reddy S. *Phys. Rev. C* 85:032801 (2012)
76. Li ZH, Schulze HJ. *Phys. Rev. C* 78:028801 (2008)
77. Pieper SC, Pandharipande VR, Wiringa RB, Carlson J. *Phys. Rev. C* 64:014001 (2001)
78. Carlson J, et al. arXiv:1412.3081 [nucl-th] (2014)
79. Sarsa A, Fantoni S, Schmidt KE, Pederiva F. *Phys. Rev. C* 68:024308 (2003)
80. Maris P, et al. *Phys. Rev. C* 87:054318 (2013)
81. Pudliner B, et al. *Physical review letters* 76:2416 (1996)
82. Gandolfi S, Carlson J, Pieper SC. *Phys.Rev.Lett.* 106:012501 (2011)
83. Carlson J, Gandolfi S. *Phys. Rev. A* 90:011601 (2014)
84. Maris P, et al. *Phys. Rev. C* 87:054318 (2013)

85. Potter HD, et al. *Physics Letters B* 739:445 (2014)
86. Bogner SK, et al. *Phys. Rev. C* 84:044306 (2011)
87. Kortelainen M, et al. *Physical Review C* 82:024313 (2010)
88. Kortelainen M, et al. *Phys. Rev. C* 85:024304 (2012)
89. Möller P, Nix JR, Myers WD, Swiatecki WJ. *At. Data Nucl. Data Tables* 59:185 (1995)
90. Carlson J, Pandharipande V, Wiringa R. *Nuclear Physics A* 401:59 (1983)
91. Tsang MB, et al. *Phys. Rev. C* 86:015803 (2012)
92. Lattimer JM, Lim Y. *The Astrophysical Journal* 771:51 (2013)
93. Gandolfi S, et al. *Eur. Phys. J. A* 50:10 (2014)
94. Hebeler K, Lattimer JM, Pethick CJ, Schwenk A. *Phys. Rev. Lett.* 105:161102 (2010)
95. Hebeler K, Lattimer JM, Pethick CJ, Schwenk A. *The Astrophysical Journal* 773:11 (2013)
96. Baym G, Pethick C, Sutherland P. *Astrophys. J.* 170:299 (1971)
97. Negele JW, Vautherin D. *Nucl. Phys. A* 207:298 (1973)
98. Lattimer JM, Prakash M. *Astrophys. J.* 550:426 (2001)
99. Heinke CO, et al. *Mon. Not. R. Astron. Soc.* 444:443 (2014)
100. Schulze HJ, Rijken T. *Phys. Rev. C* 84:035801 (2011)
101. Lonardoni D, Gandolfi S, Pederiva F. *Phys. Rev. C* 87:041303 (2013)
102. Lonardoni D, Pederiva F, Gandolfi S. *Phys. Rev. C* 89:014314 (2014)
103. Lonardoni D, Lovato A, Gandolfi S, Pederiva F arXiv:1407.4448 [nucl-th] (2014)
104. Usmani AA. *Phys. Rev. C* 52:1773 (1995)